Article

pubs.acs.org/Biomac

Polycaprolactone Microfibrous Scaffolds to Navigate Neural Stem Cells

Farrokh Sharifi,[†] Bhavika B. Patel,[‡] Adam K. Dzuilko,[‡] Reza Montazami,[†,§] Donald S. Sakaguchi,[‡] and Nastaran Hashemi*[,†,§]

[†]Department of Mechanical Engineering, [‡]Department of Genetics, Development and Cell Biology and Neuroscience, and [§]Center of Advanced Host Defense Immunobiotics and Translational Medicine, Iowa State University, Ames, Iowa 50011, United States

Supporting Information

ABSTRACT: Fibrous scaffolds have shown promise in tissue engineering due to their ability to improve cell alignment and migration. In this paper, poly(ε-caprolactone) (PCL) fibers are fabricated in different sizes using a microfluidic platform. By using this approach, we demonstrated considerable flexibility in ability to control the size of the fibers. It was shown that the average diameter of the fibers was obtained in the range of 2.6−36.5 μm by selecting the PCL solution flow rate from 1 to 5 μL min^{-1} and the sheath flow rate from 20 to 400 μL min^{-1} in the microfluidic channel. The microfibers were used to create 3D microenvironments in order to investigate growth and differentiation of adult hippocampal stem/progenitor cells (AHPCs) in vitro. The results indicated that the 3D topography of the PCL substrates, along with chemical (extracellular matrix) guidance cues supported the adhesion, survival, and differentiation of the AHPCs. Additionally, it was found that the cell deviation angle for 44−66% of cells on different types of fibers was less than 10°. This reveals the functionality of PCL fibrous scaffolds for cell alignment important in applications such as reconnecting serious nerve injuries and guiding the direction of axon growth as well as regenerating blood vessels, tendons, and muscle tissue.

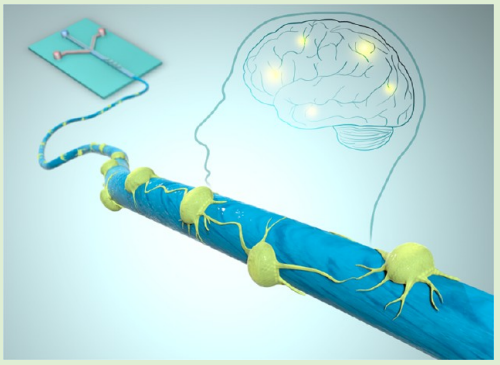

1. INTRODUCTION

Tissue engineering is an interdisciplinary area that combines engineering and biology in order to improve or replace biological functions.[1,2] This area can be equipped by microfabrication methods, which are powerful tools with extremely high potential to handle some of the obstacles in tissue engineering.[3] In most applications, scaffolds are made of biomaterials and applied in order to provide a suitable 3D environment with intentions toward controlling cell behavior, such as adhesion, proliferation, differentiation, migration, alignment, and in providing efficient nutrient transport as well as sufficient mechanical properties.[4,5] However, there are some challenges in tissue engineering; the biomaterial must be compatible with the cells in question in order to sustain reasonably normal behaviors. As such, it is essential to gain a better understanding of the microenvironmental conditions required to regulate the cells fate. Additionally, tissue engineering suffers from a lack of biomaterials with desirable biological, chemical, and mechanical properties.[4] To meet this need, enormous efforts have been made to discover new biomaterials and to study the biocompatibility and biodegradability of different materials.[6,7]

A prominent area of tissue engineering is related to regenerative medicine and neurorepair. The discovery of effective therapeutic interventions targeted toward neurodegenerative conditions and nerve injuries has proven challenging. Scientists and engineers have been drawn into the field of neural tissue engineering due to its importance for development of novel therapeutic strategies. For example, peripheral nerve regeneration is a complicated phenomenon which is often successful as long as the injuries are small. With more severe nerve injuries such as a nerve gap, however, interposition of a nerve graft or nerve regeneration conduit is usually required. Complexity in spinal cord injury is more serious since, for the most part, regeneration is prohibited. Fortunately, neural tissue engineering provides extraordinary promise to combat this central nervous system (CNS) injury.[8] For example, Hurtado et al. demonstrated axonal regeneration within a spinal cord injury using aligned poly-L-lactic acid microfibers.[9] Microfibers may provide a supportive environment for a recovering nervous system due to the combination of physical and biological cues.

Microfibers have been fabricated for neural tissue engineering using different approaches such as microfluidics, electrospinning, and wet spinning.[10−19] Agarwal et al. reported some of the studies in electrospinning fiber fabrication technique for biomedical applications such as tissue engineering and drug delivery.[20,21] Polycaprolactone (PCL) is one of the biocompatible and biodegradable polymers applied for the fibers fabricated in this technique.[21−30] Schnell et al. showed that

Received: July 8, 2016
Revised: August 31, 2016
Published: September 6, 2016

DOI: 10.1021/acs.biomac.6b01028
Biomacromolecules 2016, 17, 3287−3297

using electrospun PCL and collagen/PCL fibers can significantly improve the attachment, migration, and neurite orientation of Schwann cells.[21] In addition to PCL, other biocompatible polymers have been used in nerve tissue engineering such as gelatin and polylactic acid (PLA).[16,17] However, accurately aligning the fibers in electrospinning method is difficult.[16,22,31] This method is not functional for cell encapsulating purposes due to the fact that the size of the fibers are mostly limited to nanoscales. Furthermore, high voltages (5−50 kV) need to be applied for pulling the charged solution, which might damage sensitive biological materials.[32] Wet spinning method has been employed in nerve tissue engineering as well. Siriwardane et al. fabricated collagen fibers and treated them by cross-linkers glutaraldehyde and genipin in order to improve the mechanical properties and decrease swelling.[15] In wetspinning, the sample is exposed to chemicals and osmotic gradients for a relatively long time, which can have detrimental effects on the cells.[33,34] Additionally, the cross section of the fibers made by electrospinning and wetspinning are mostly round due to the surface tension in the two-phase systems of liquid/air and immiscible liquid/liquid, respectively.[35]

Microfluidics is an interdisciplinary field that has received much attention, mostly because of its wide applications from energy systems to biomedical areas.[36−39] Microfluidic fiber fabrication, which is the newest approach, retains most advantages of other fiber fabrication approaches and minimizes some of their shortcomings. One of the important features of using microfluidic fiber fabrication is the compatibility with cells, proteins, drugs, and peptides as well as versatility, cost-effectiveness, and simplicity.[5,40−42] In this method, there is no need to apply high temperature, high pressure, and high voltages.[5,40,43−46] This approach makes it feasible to fabricate fibers with different shapes of solid,[13,47−50] tubular,[51,52] hybrid,[31] and flat[14,53,54] dimensions for divergent applications such as cell encapsulation, alignment, and immobilization.

In terms of material, there are both synthetic and natural biodegradable and biocompatible polymers. We used PCL, a synthetic polymer, in this study. Synthetic polymers have some advantages over the natural materials. For example, the polymer composition can be accurately controlled such that a wide range of properties is obtainable for the synthetic polymers. In addition, they are more uniform with sufficient source of raw materials.[55,56] Comparing with other synthetic polymers, such as PLGA, PCL has slower degradation rate, which makes it less acidic during degradation and desirable for long-term implantable devices. Although some studies focused on using the PCL electrospun fibrous scaffolds in nerve tissue engineering, there is no report on employing hydrodynamic focusing (microfluidic approach) and solvent extraction to fabricate biocompatible PCL fibers in nerve regeneration tissue engineering.[57−59] In this paper, we show that microfluidic fiber fabrication may be used as a scalable and widely accessible alternative technique to fabricate PCL fibrous scaffolds with tuned characteristics to enhance the growth and differentiation of neural stem cells as well as neurite orientation. We cultured green fluorescent protein-expressing (GFP) adult hippocampal stem/progenitor cells (AHPCs) on PCL microfibers and investigated their ability to adhere, survive, proliferate and differentiate. AHPCs were used because of their ability to differentiate into the fundamental cells of the CNS. In order to study CNS regeneration therapies, it is important to consider the population of cells needed for repair of a damaged nervous system. The AHPCs were maintained in medium supplemented with bFGF and upon growth factor withdrawal, these multipotent AHPCs differentiated into neurons and glial cells.[60,61] Neurons are able to transmit information and are the key cells of the nervous system, whereas glial cells serve as the support cells of the CNS. The microfluidic microfabrication platform was able to create a biocompatible scaffold out of fibers to provide a desirable growth environment for the neural stem cells. We showed that the cells attach to and align themselves on the microfiber substrates. In this study, cell death was minimal, and cell proliferation was affected by changing the features of the fibrous scaffold. Ideally, as the scaffold is degraded a more natural microenvironment is created by the cells and the production of their extracellular matrix (ECM), thus resulting in a bioengineered 3D network that mimics the native tissue.

2. EXPERIMENTAL SECTION

Materials. Poly(ε-caprolactone) (PCL) (M_n = 80 000), polyethylene glycol (PEG) (M_n = 20 000), and ethanol were purchased from Sigma-Aldrich (St. Louis, MO). 2,2,2-Trifluoroethanol (TFE), which is the solvent for PCL, was obtained from Oakwood Chemical (West Columbia, SC).

Microfluidic Channel. A SU8 photoresist-patterned silicon wafer was applied as a mold and the channel was made using soft lithography. We used two silicon wafers in order to create the pattern of the microchannel and the chevron grooves extended from two sides of the channel. The dimensions of the microchannel are 130 μm × 390 μm (height × width). The microchannel has four diagonal grooves with dimensions of 130 μm × 100 μm (height × width) and are spaced 200 μm apart. Polydimethylsiloxane (PDMS), which is a biocompatible and transparent elastomer, was made from the mixture of Sylgard 184 elastomer base and cross-linker agents in a 10:1 ratio. Then, the mixture was poured onto the mold, and cured with the temperature of 85 °C for 25 min. After that, the PDMS layer on the silicon wafers were peeled off and the layers were bonded together using plasma treatment.

Microfluidic Fiber Fabrication. The 5 wt % PCL solution (core fluid) was obtained by mixing 1 g of PCL in 20 mL TFE at room temperature. The sheath solution was prepared by adding 1 g of PEG in 20 mL mixture of ethanol and deionized (DI) water with a volume ratio of 1:1 to prepare 5 wt % PEG solution. These two solutions were introduced into the microchannel via a double syringe pump (Cole-Parmer, Veron Hillss, IL) with different flow rate ranges of 2−5 μL min^{-1} and 10−120 μL min^{-1} for the core and sheath solution, respectively. Using this method, the fibers remain aligned after fabrication. The microchannel was vertically positioned into a water bath, and the resulting fibers were gathered around a paper frame in an aligned manner (Figure S1a).

Cell Culture. Adult hippocampal progenitor cells (AHPCs) were originally isolated from adult Fischer 344 rats and infected with a retrovirus to express green fluorescence protein (GFP) as described previously and were a generous gift from F. H. Gage (Salk Institute for Biological Sciences, La Jolla, CA).[62] Cells were grown in flasks coated with poly-L-ornithine (10 μg mL^{-1}; Sigma-Aldrich) and purified mouse laminin (5 μg mL^{-1}; R&D Systems) in Earle's balanced salt solution (EBSS). Maintenance media (MM) included Dulbecco's modified Eagle's medium/Ham's F-12 (DMEM/F-12, 1:1; Omega Scientific), supplemented with 2.5 mM L-glutamine, N2 supplement (Gibco BRL), and 20 ng mL^{-1} basic fibroblast growth factor (human recombinant bFGF; Promega Corporation). The AHPCs were detached from flasks using 0.05% trypsin−EDTA (Gibco BRL) and harvested by centrifugation at 800 rpm for 5 min. A hemocytometer was used to perform a Trypan Blue viable cell count, and AHPCs were plated at a density of 10 000 cells/cm^2 on PCL-microfiber substrates (see below). Cells were maintained at 37 °C in a 5% CO_2/95% humidified air atmosphere. For cell differentiation, AHPCs were cultured in growth medium lacking bFGF (referred to as differ-

DOI: 10.1021/acs.biomac.6b01028
Biomacromolecules 2016, 17, 3287−3297

Scheme 1[a]

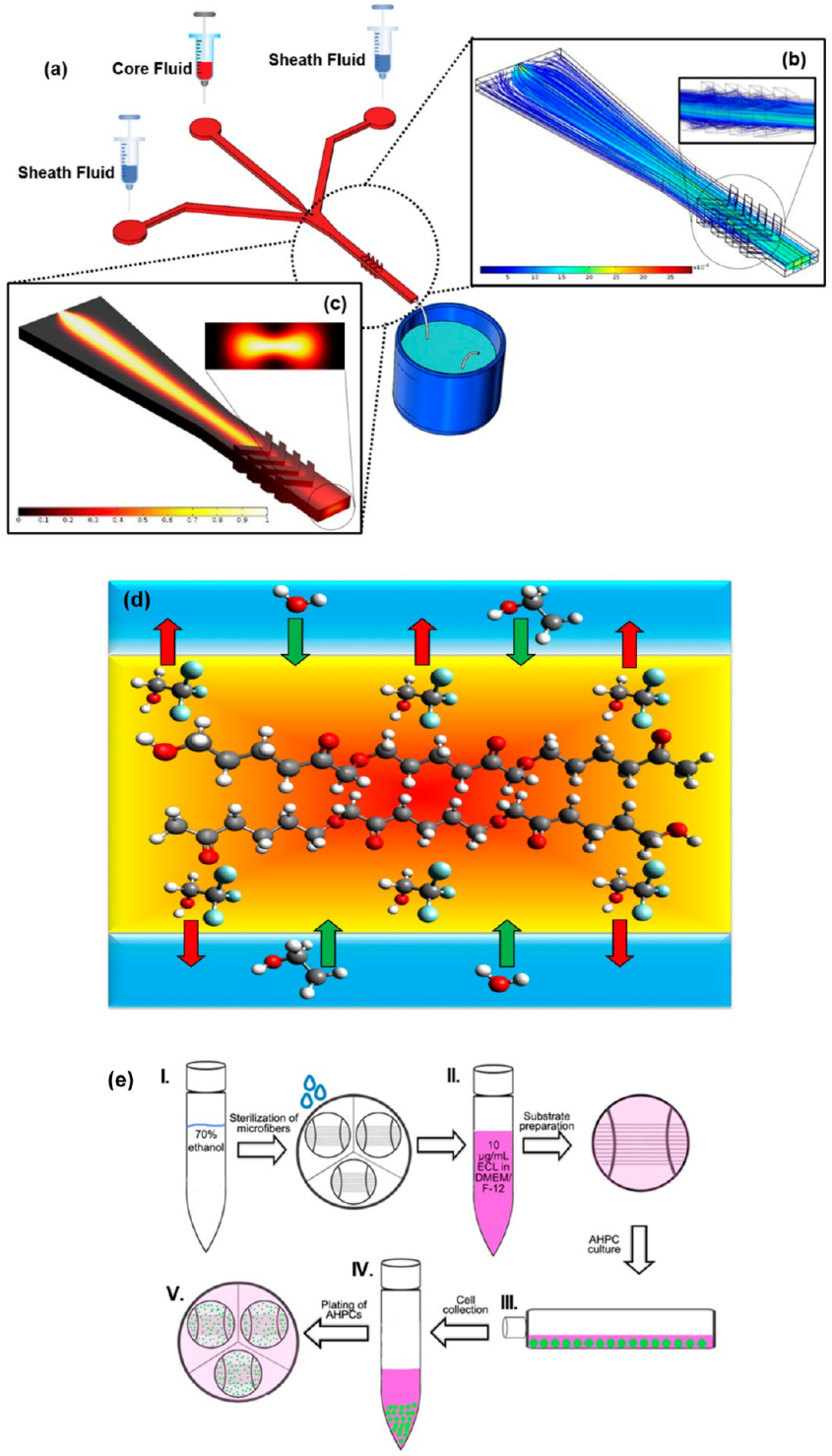

[a](a) Schematic of the microfluidic fiber fabrication. (b) Streamline and velocity (m s^{-1}) of the fluids along the channel. (c) Illustration of concentration profile (mol m^{-3}): the dark and bright colors represent the sheath and core fluids, respectively. (d) Phase inversion process: the TFE molecules are replaced with the molecules of the sheath fluid, which results in PCL solidification. (e) Cell culture procedure: (I) Sterilization of microfibers on coverslips using 70% ethanol for 20 min; (II) diluted ECM substrate (ECL) in DMEM/F-12 to a final concentration of 10 μg mL^{-1}; (III) culture AHPCs in T-75 flask until 80% confluent; (IV) apply trypsin to cells for collection; and (V) culture cells on ECL-coated microfibers in differentiation media for 7 days.

entiation medium, DM) for 7 days. Half of the media was changed every other day.

Substrate Preparation. Glass coverslips (12 mm, Fisher Scientific) were cleaned using RBS 35 (Thermo Scientific) detergent diluted (1:50) in deionized water and boiled for 15 min. Coverslips were then rinsed in DI water, air-dried and ultraviolet light was used for sterilization. The microfibers were then attached to the coverslips using medical adhesive. Small droplets of medical adhesive were placed

DOI: 10.1021/acs.biomac.6b01028
Biomacromolecules 2016, 17, 3287−3297

at opposite sides of the coverglass and a parallel array of microfibers placed across the coverglass and attached to the medical adhesive droplets. Small chip of coverglass were then used to secure the microfibers to the coverglass. The microfibers were fixed at opposite ends and loose across the middle of the coverglass (Figure S1b). The coverglass and PCL-microfiber substrates were sterilized by incubation in 70% ethanol for 20 min and rinsed with Earle's balanced salt solution (EBSS; Invitrogen). After 10 min of air-drying, the microfiber substrates were incubated at 4 °C overnight with Entactin-Collagen IV-Laminin (ECL; Millipore) at 10 μg mL^{-1} in DMEM/F-12 to facilitate cell attachment. The next day, the ECL was removed, samples were rinsed with EBSS, and cells plated.

Immunocytochemistry. After 7 days of culturing in DM, the cells were rinsed with 0.1 M phosphate ($P0_4$) buffer and immediately fixed with 4% paraformaldehyde (PFA) in 0.1 M $P0_4$ buffer for 20 min at room temperature. PFA was removed and rinsed with phosphate buffer saline (PBS; Invitrogen) and incubated in blocker solution (PBS supplemented with 5% normal donkey serum (Jackson ImmunoResearch), 5% normal goat serum (Jackson ImmunoResearch), 0.4% bovine albumin serum (Sigma), and 0.2% Triton X-100 (Fisher Scientific)) at room temperature for 1 h. Primary antibodies (see Table S1 for list of primary antibodies) were diluted in blocker solution and samples incubated at 4 °C overnight. On the following day, antibodies were removed and samples were rinsed with PBS. Secondary antibodies, donkey anti-rabbit Cy3 and donkey anti-mouse Cy3 (Jackson ImmunoResearch), were diluted in blocking solution at a dilution of 1:500 along with the nuclear stain, DAPI (1:50, Invitrogen). Samples were incubated in secondary antibody/DAPI solution for 90 min at room temperature. Samples were then mounted on microscope slides using DAPI Fluoromount-G (Southern Biotech) mounting media and stored at 4 °C until imaging.

Propidium Iodide Staining. Propidium iodide (PI) was used to measure cell death/survival at 7 days in vitro. Propidium iodide stain solution was prepared at a concentration of 1.5 μM in culture medium. Half of the samples served as the positive, reagent control for the PI stain and subjected to 70% ethanol for 5 min to induce cell death. The ethanol and MM were removed from all samples and the culture media containing PI was added for 20 min at 37 °C in a 5% CO_2 incubator. The samples were then rinsed with 0.1 M $P0_4$ buffer, fixed with 4% PFA, and rinsed again with PBS. Samples were then incubated with DAPI (1:50) diluted in blocker solution for 1 h at room temperature. Following PBS rinses, samples were mounted on microscope slides using DAPI Fluoromount-G mounting media and stored at 4 °C until imaging.

Imaging and Measuring the Alignment Angles. Fluorescent images were conducted using a fluorescence microscope (Nikon Microphot FXA, Nikon, Inc.), equipped with a Retiga 2000R digital camera controlled by QCapture software (QImaging). Images were pseudocolored using Adobe Photoshop CC. Table S1 provides information about the different antibodies applied for studying AHPC growth on the microfibers. Scanning electron microscopy (SEM; JCM-6000 NeoScope Benchtop scanning electron microscope) was applied to study the size, morphology, and deviation angle of the fibers and cells. In order to acquire high quality SEM images, the substrates were made conductive using gold sputter-coating. The coating thickness of the samples was around 50 nm. The cell and fiber deviation angles were measured using the SEM images and ImageJ, which is an imaging analysis software. For the fiber size and deviation angle, around 30 fibers were studied, whereas the positions of around 100 cells were evaluated relative to the fiber direction in each type of fiber.

3. RESULTS AND DISCUSSION

Two fluids, i.e., the core and sheath fluids, are introduced into the microchannel and diffusion occurs only at the core/sheath fluid interface due to the laminar flow regime. In order to have a continuous fiber fabrication process, a core/sheath flow profile is required.[5] Scheme 1a provides a schematic picture of the microfluidic fiber fabrication. The sheath fluid focuses the

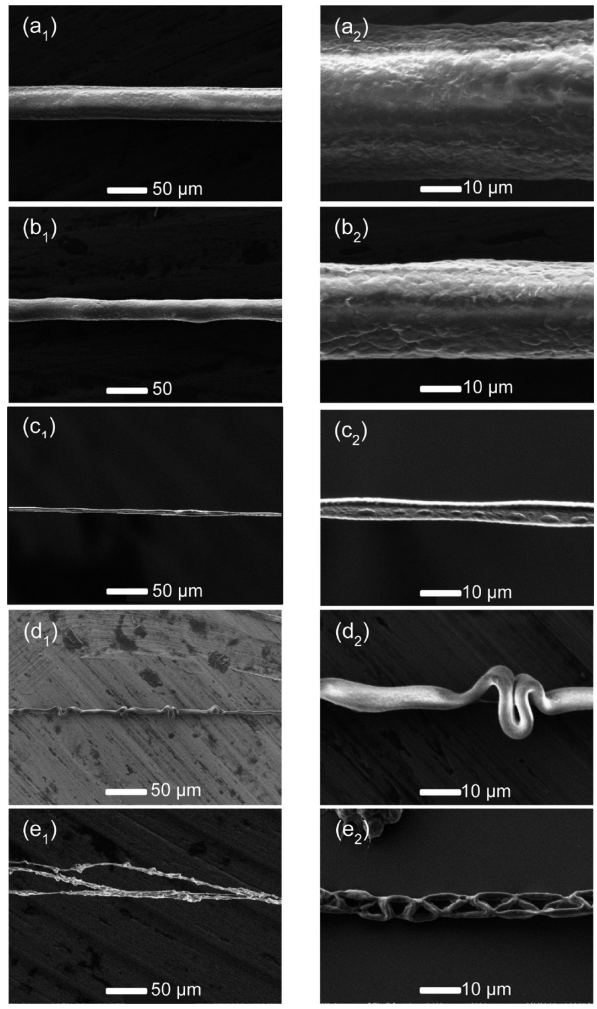

Figure 1. SEM images of the microfluidic spun PCL microfibers at different sheath-to-core flow rates of (a) 20:5, (b) 60:5, (c) 200:4, (d) 300:2, and (e) 400:1. The concentrations of the PCL and PEG are 5% in TFE and water/ethanol, respectively.

core fluid laterally after the two fluids are introduced at the upstream of the channel and changes the shape of the core fluid to a thin vertical strip. Chevron grooves in the downstream of the channel decrease the hydrodynamic resistance perpendicular to the flow direction. The sheath flow rate is higher than the core flow rate in order to provide the force needed to keep the core fluid at the center of the microchannel. Because the hydrodynamic resistance is inversely proportional to flow rate, the sheath fluid fills the grooves, wraps around the core fluid, and pushes it to the center of the channel.[63−65] The streamline and velocity distribution of the fluids along the channel are provided in Scheme 1b. Scheme 1c demonstrates the concentration profile through the channel. The dark and bright colors show the sheath and core fluids, respectively. These figures clearly illustrate the role of the sheath fluid and chevron grooves to exert the lateral and vertical hydrodynamic focusing forces on the core fluid. The lateral and vertical hydrodynamic focusing forces, which are originated from the shear force between the core and sheath fluids, play a pivotal role to keep the core fluid at the center, align the polymer chain, and change the shape of the microfibers. The hydrodynamic force depends on the viscosity and relative velocity of the core and sheath fluids. By adding polyethylene glycol (PEG) to the sheath fluid,

DOI: 10.1021/acs.biomac.6b01028
Biomacromolecules 2016, 17, 3287−3297

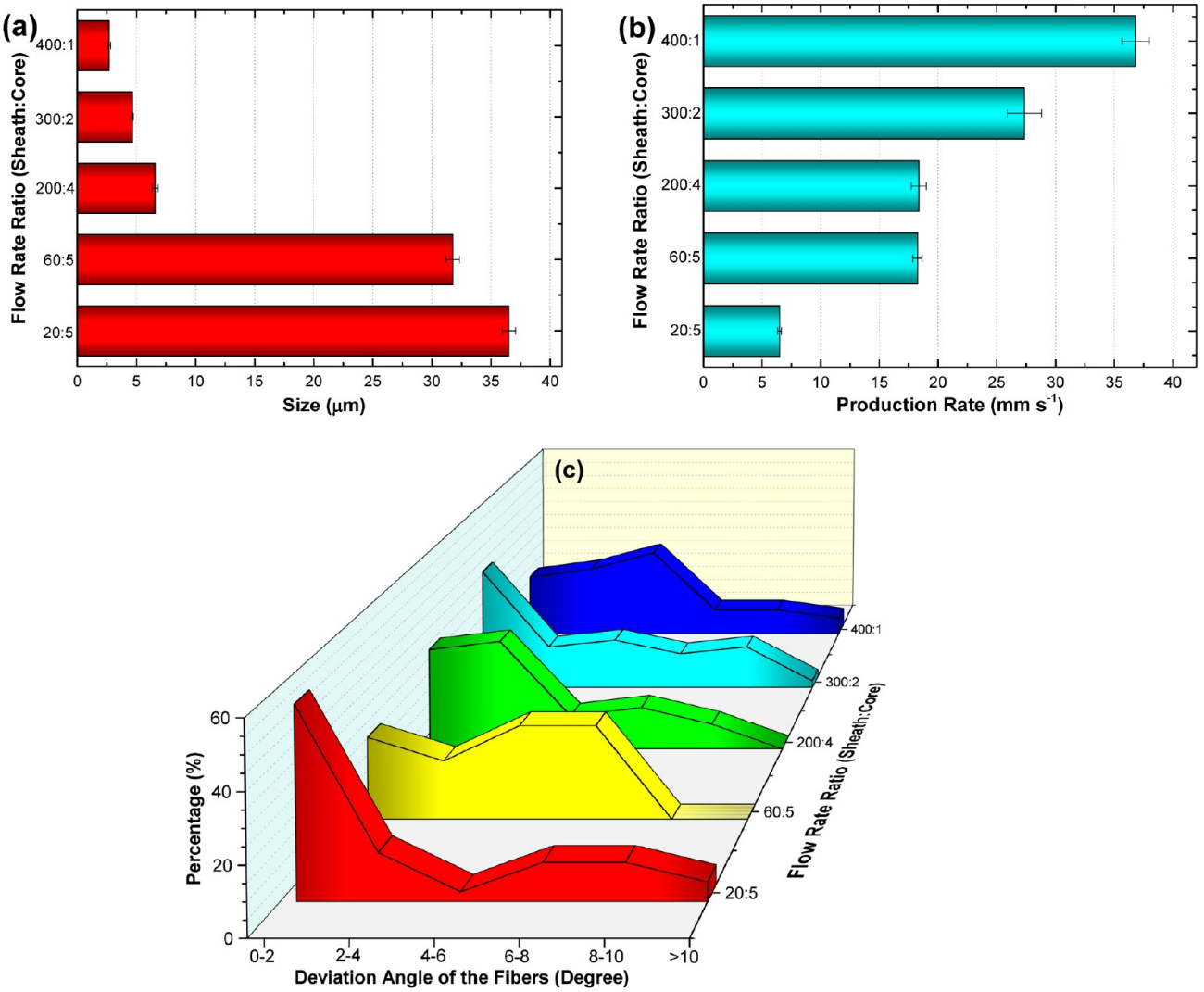

Figure 2. Characteristics of the PCL microfibers: (a) size, (b) production rate, and (c) alignment of the fibers fabricated using different sheath-to-core flow rate ratios.

the viscosity of core and sheath solutions match and there is no need to use high relative velocities to focus the core fluid when fabricating the fibers. Additionally, there is a possibility of flow instability in the channel at high relative velocities that results in changing the flow regime to transient from laminar.

Phase inversion (solvent extraction) strategy was used to solidify PCL and fabricate microfibers. In this process, 2,2,2-trifluoroethanol (TFE) in the core fluid is replaced by the ethanol and water in the sheath fluid at the interface between the sheath and core solution (Scheme 1d). This exchange results in PCL solidification because the sheath fluid is miscible to TFE, but not solvent to PCL. Scheme 1e describes the sterilization and cell culture protocol for AHPCs. Following the plating of AHPCs, cells are incubated for 7 days in differentiation media, and subsequently fixed and immunolabeled for further analysis.

Figure 1 shows the SEM images of the fibers fabricated using the flow rate ranges of 1−5 μL min^{-1} and 20−400 μL min^{-1} corresponding to the core and sheath fluids, respectively. The concentration of the PCL in TFE and PEG in the water/ethanol were kept at a constant value of 5%. In the phase inversion solidification process, used to solidify the PCL fibers, the molecules of TFE are replaced by the molecules of the sheath fluid. Due to this diffusion at the fluid/fluid interface, the surface of the PCL fibers are not smooth, which could provide a better environment for the cells to adhere to the surface of the fibers. Additionally, this figure shows consistency with the theory of hydrodynamic focusing meaning that when the flow rate ratio between the core and sheath fluids decreases, the shear force at the interface exerted from the sheath fluid to the core fluid weakens. Therefore, the core fluid extends in the channel and the size of the resulting fiber increases. This figure also demonstrates that once the flow rate ratio exceeds 50, the fibers will not be smooth anymore. This condition continues until the wavy fibers connect with each other and create a chain, that could be considered as a self-assembly structure (Figure 1e). This was expected because when the flow rate ratio between the fluids increases, the sharp velocity gradient at the fluid/fluid interface intensifies the shear force, which decreases the flow stability and the regime starts to lie in the transition region.[45] The average size and production rate of the fibers (mean ± standard error) are shown in Figure 2a and b, respectively. The results show that the diameters of the fibers lie in the range of 2.6−36.5 μm, which can be obtained by changing the sheath-to-core flow rate of 400:1−20:5, respectively. This figure demonstrates the capability of the

DOI: 10.1021/acs.biomac.6b01028
Biomacromolecules 2016, 17, 3287−3297

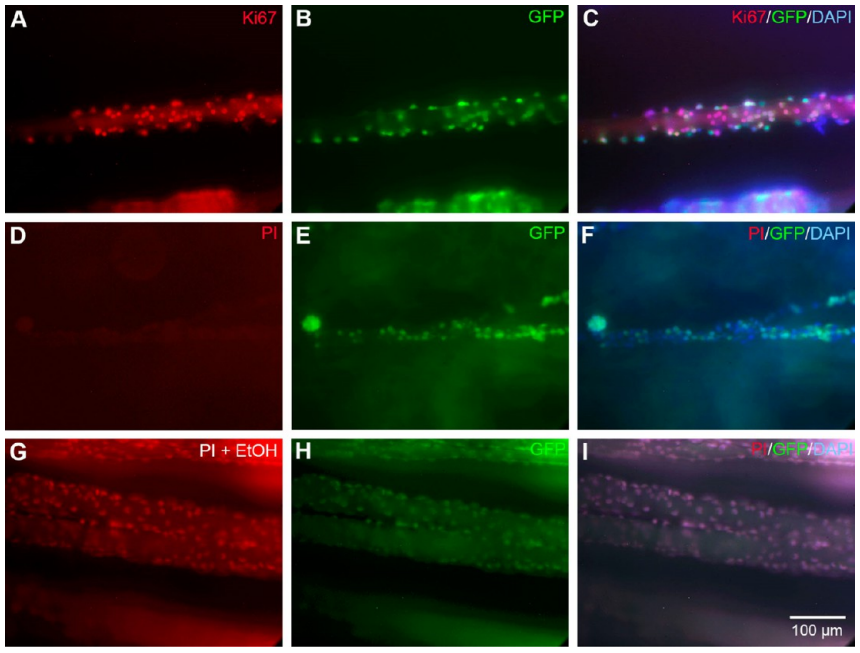

Figure 3. Proliferation and survival of AHPCs cultured on PCL microfibers. Fluorescence images of AHPCs immunolabeled for *Ki*-67, cell proliferation marker (A–C) or propidium iodide (PI) staining. Middle column of images illustrate GFP-expressing AHPCs (B, E, and H). As a control for the PI staining reagents, samples were subjected to ethanol (EtOH) treatment that causes most cells to die resulting in extensive PI-staining (G, H, and I). Merged images (C, F, and I) of antibody labeling or PI-staining (red) with GFP-expression (green) and DAPI nuclei counterstaining (blue). Scale bar = 100 μm.

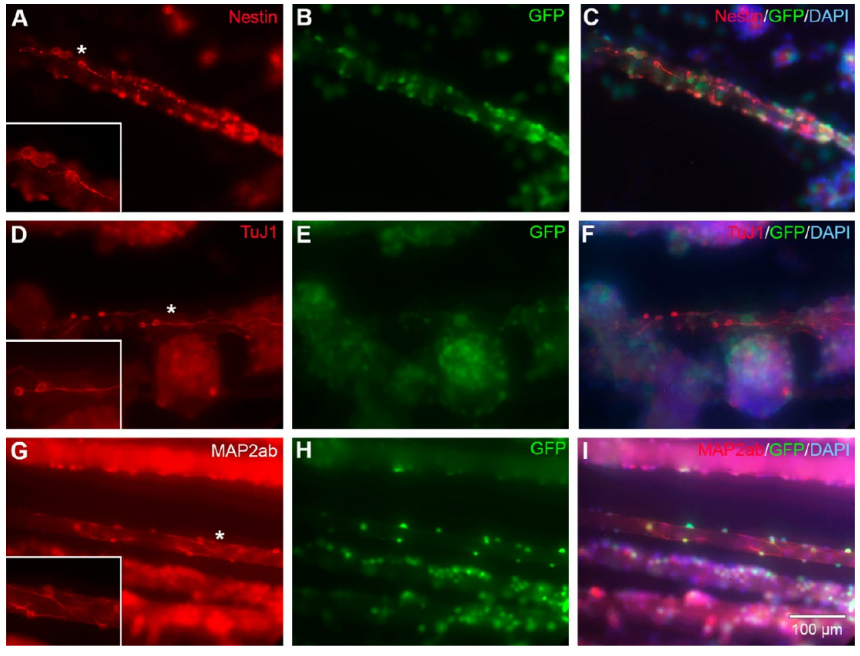

Figure 4. Attachment and differentiation of AHPCs cultured on PCL microfibers. Fluorescence images of AHPCs immunolabeled for nestin (A–C), TuJ1 (D–F), and MAP2ab (G–I). Middle column of images illustrate GFP-expressing AHPCs (B, E, and H). Merged images (C, F, and I) of antibody labeling (Cy3, red) with GFP-expression (green) and DAPI nuclei counterstaining (blue). Asterisks indicate the location of the higher magnification inset images in (A), (D), and (G). Attachment of cells is seen through immunolabeling of processes around microfibers. Scale bar = 100 μm (200 μm for insets).

microfluidic fiber fabrication in tuning the size of the fibers by simply changing the flow rate ratio between the sheath and core fluids. As expected, the production rate of the fiber directly depends on the sheath and core flow rates. The maximum production rate was 37 mm s^{-1} for the sheath-to-core flow rates of 400:1, and it decreases to 6.5 mm s^{-1} when the sheath-to-core flow rate of 60:5 is used. However, it does not mean that the range of the production rate in microfluidic approach is limited. We can increase the production rate by increasing the sheath and core flow rates. However, in this study, we mostly focused on studying the alignment of the AHPCs on fibers with different sizes. The small error bars reveal the uniformity of the

DOI: 10.1021/acs.biomac.6b01028
Biomacromolecules 2016, 17, 3287–3297

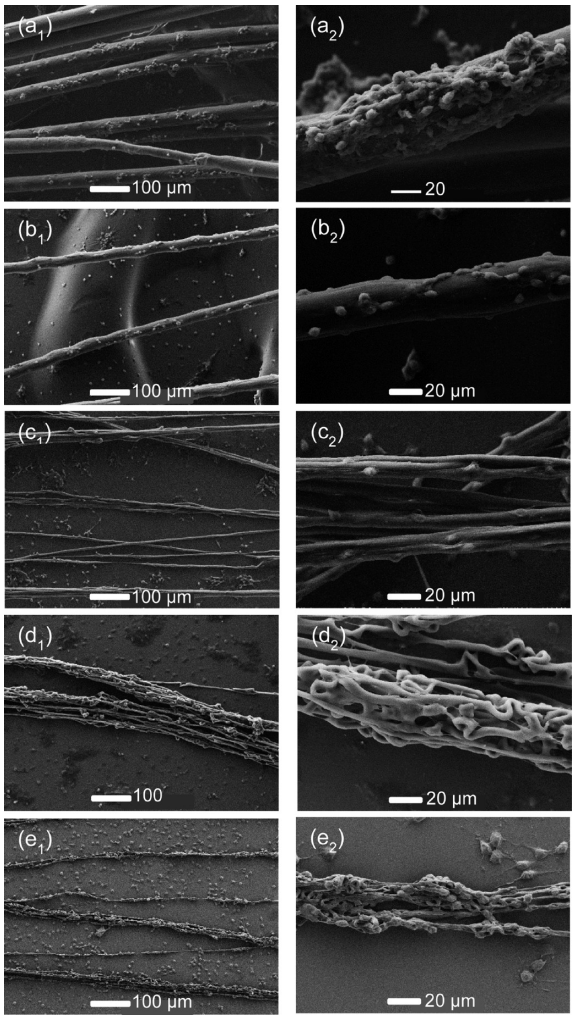

Figure 5. SEM images of the AHPCs growing on PCL microfibrous scaffolds fabricated by using different sheath-to-core flow rates of (a) 20:5, (b) 60:5, (c) 200:4, and (d) 300:2. PCL and PEG concentrations are 5% in TFE and water/ethanol, respectively.

size and production rate of the fibers made by this method. Figure 2c illustrates the alignment of different types of fibers by presenting the percentage of fiber deviation angle, i.e., the angle between each one of the fibers and a reference. This figure shows that the percentage of the fibers with fiber deviation angle larger than 10° are 5.55%, 0%, 0%, 2.38%, and 6.1% for the sheath-to-core flow rates of 20:5, 60:5, 200:4, 300:2, and 400:1, respectively. This shows one of the advantages of microfluidic approach over common fiber fabrication methods, which is the feasibility of this method to simply fabricate the aligned fibers.

Ki-67 immunolabeling was used to evaluate whether the PCL microfibers would support proliferation of the AHPCs. Expression of the *Ki*-67 antigen occurs during the cell cycle (not detected in cells in the resting phase) and therefore is commonly used as a cellular marker for cell proliferation. *Ki*-67 immunolabeled cells were present on all microfibers examined. Figure 3A–C illustrates an example of *Ki*-67 immunolabeled cells growing on microfluidic spun PCL microfibers at a sheath-to-core flow rate of 60:5. The results of proliferation of AHPCs on all types of fabricated fibers are provided in Figure S2. Propidium iodide staining was used to evaluate survival of AHPCs growing on the microfibers (Figure 3D–I). Propidium iodide is a fluorescent nuclear and chromosome counterstain that is membrane impermeant and commonly used to identify dead cells in a population.

Figure 3D–F shows that very few PI-positive cells were detected in the microfiber cultures. In contrast, as a positive control for the PI reagents, some samples were subjected to 70% ethanol, a condition that kills most cells, resulting in the majority of cells PI-labeled (Figure 3G–I). It is notable that the cells remained attached following the 70% ethanol treatment. This is likely due in part to the immediate fixation in paraformaldehyde. Furthermore, the ECL substrate absorption onto the PCL microfibers facilitates cell attachment. Taken together, the *Ki*-67 immunolabeling and Propidium Iodide staining results indicate that the different PCL microfibers produced by the different sheath-to-core flow rates all supported adhesion and cell proliferation, and did not dramatically affect cell viability.

AHPCs growing on the different PCL microfibers were characterized morphologically and immunocytochemically using a panel of cell-type specific antibodies (Table S1). The AHPCs are a multipotent population of adult neural stem cells and have the capacity to differentiate into neurons, oligodendrocytes and astrocytes.[61] The phenotypes of AHPCs growing on the microfibers were assessed using antibodies directed against nestin, an intermediate filament protein present in neural stem/progenitor cells; class III β-tubulin (TuJ1), a protein characteristic of early neurons; microtubule-associated protein 2ab (MAP2ab), characteristic of maturing neurons; and the glial markers, receptor interacting protein (RIP) and glial fibrillary acidic protein (GFAP), for oligodendrocytes and astrocytes, respectively. AHPCs were identified in culture based on green fluorescent protein GFP-expression and counterstaining with DAPI allowed visualization of the cell nuclei. Many of the AHPCs were immunolabeled with the nestin, TuJ1 and MAP2ab antibodies (Figure 4), fewer cells were immunoreactive for the glial markers RIP and GFAP (Figure S3). Figure 4 illustrates examples of AHPCs growing on microfluidic spun PCL microfibers at a sheath-to-core flow rate of 300:2 that were immunolabeled with the nestin (Figure 4A–C), TuJ1 (Figure 4D–F), or MAP2ab (Figure 4G–I) antibodies. Nestin, a marker for multipotent neural stem cells, has important functions in the survival and self-renewal of NSCs. AHPCs immunolabeled for nestin indicates that many of the cells growing on the PCL microfibers retained their progenitor-like status. Under differentiation conditions (initiated by growth factor withdrawal) AHPCs begin differentiating and many cells were immunolabeled with the neuronal markers TuJ1 and MAP2ab. Immunolabeled cells displayed neuronal morphologies, often exhibiting longer neurites of various lengths on the microfiber surface. Though all three antibody markers (nestin, TuJ1, and MAP2ab) label different cytoskeletal elements, all are expressed within the cytoskeleton of the neurite processes as was clearly evident in the fluorescent images (Figure 4). It was noted that some of the AHPCs undergo a decrease in expression of GFP during the course of cell culture, indicating a down regulation of the GFP transgene during the course of establishment of stable cell populations that allow long-term culture. However, these low GFP expressing AHPCs continued to survive, proliferate, and differentiate in a normal fashion.

The SEM images of AHPCs on the PCL microfibers are shown in Figure 5. This figure illustrates that most of the cells can be aligned to the longitudinal direction of the fibers with

DOI: 10.1021/acs.biomac.6b01028
Biomacromolecules 2016, 17, 3287–3297

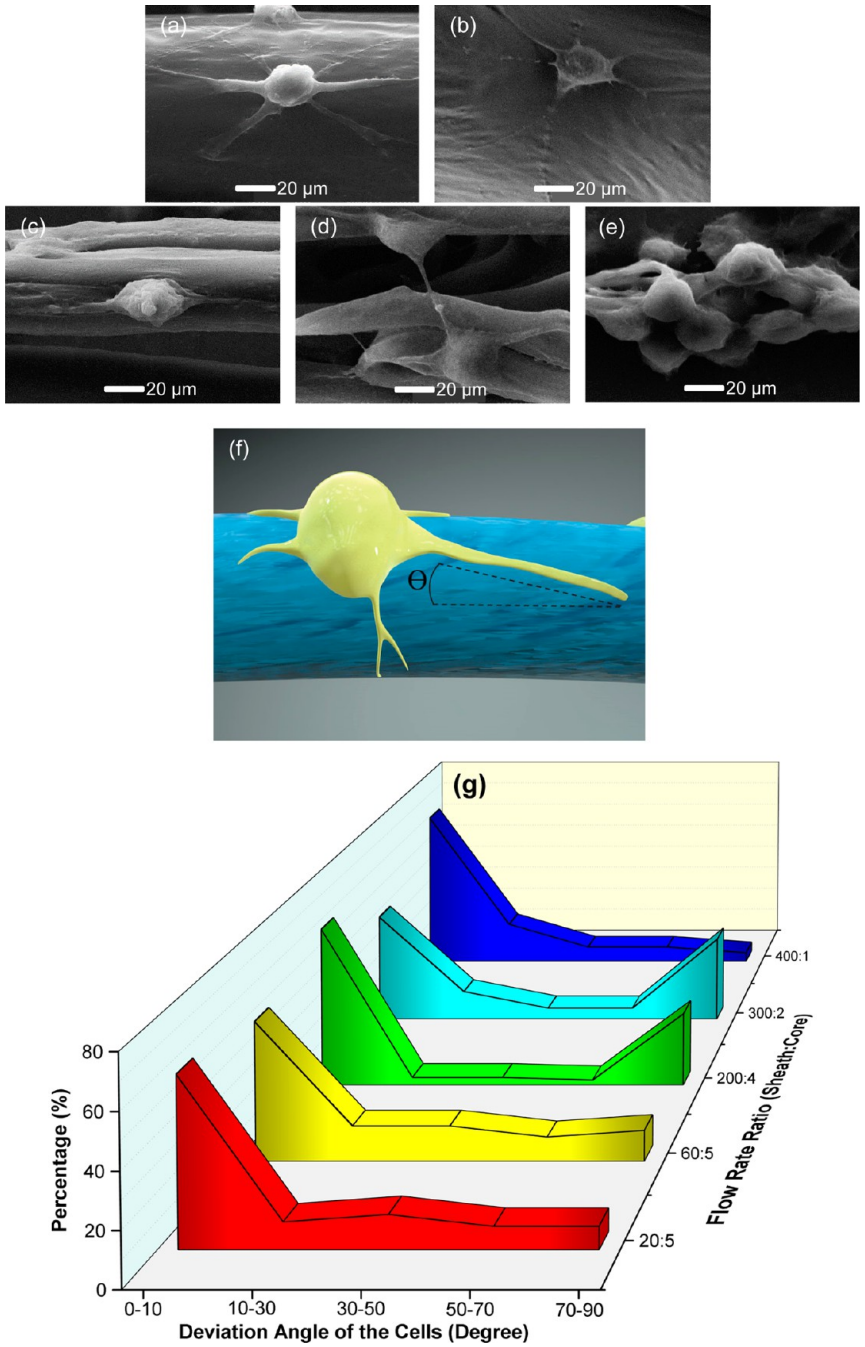

Figure 6. (a–e) SEM images of the AHPCs cultured on the PCL microfibers. (f) Illustration of cell deviation angle. (g) Quantification of the neurite orientation on the fibers.

different sizes. This reveals the role of the fibers as scaffolds to be applied for supporting the proliferation and differentiation of AHPCs. However, the fibers with larger sizes can physically support more cells on their surfaces compared to smaller ones. The SEM images with higher magnifications are provided in Figure 6a–e. In terms of the size of the aligned PCL fibers, this figure shows that while the predominant alignment of the cells is in the axial direction of the fibers, the cells on fibers with the average size of 4–7 μm on occasion bridged from one fiber to another one (Figure 6d). The likely reason for such behavior is that the distance between the thinner fibers is shorter and that bundles of fibers have been created. As a result, the cell can bridge between two fibers. However, Figure 6e demonstrates that this behavior is not observed for the thinnest fiber. That is because the fibers are wavy (Figure 1e) due to the large velocity difference between the core and sheath fluids and resulting instability. It is possible that when placed in cell culture, the fibers become braided such that it is more difficult to separate the fibers from each other. When the fibers with the flow rate ratio of 400:1 are braided, a uniform bundle is created which allows more cells to attach on the surface due to increase surface area. Additionally, the empty space between the fibers may mimic a 3D microenvironment for the cells in order to allow nutrients to be exchanged to increase survival of cells. It can be observed that although this type of fiber are wavy and develop in different directions, the ultimate direction of all of

DOI: 10.1021/acs.biomac.6b01028
Biomacromolecules 2016, 17, 3287–3297

the fibers are in the same direction. However, it was reported that the mechanical properties of the PCL fibers decrease with increasing flow rate ratio.[45] Therefore, if high mechanical properties are required, larger fibers are better choices for the PCL fibrous scaffolds that provide enough strength as well as a desirable microenvironment for aligning the cells. The neurite orientation on the fibers was analyzed quantitatively based on SEM images by measuring the cell deviation angle, which is the angle between the main axis of the cells and the fibers (Figure 6f). The results of measuring the cell deviation angle are shown in Figure 6g. This figure demonstrates that the cell deviation angle is mostly less than 10° for fibers with different sizes, which reflects that the PCL microfibers were able to align the AHPCs efficiently along their axial directions. The percentage of the cells with deviation angle lower than 10° is 61%, 53%, 63%, 44%, and 66% for the fibers fabricated using the sheath-to-core flow rate ratio of 20:5, 60:5, 200:4, 300:2, and 400:1, respectively. The percentage of the cells with deviation angle larger than 10° decreases significantly. However, number of the cells with the cell deviation angle in the range of 70−90° increases to the maximum values of 29% and 35% on the fibers made by the sheath-to-core flow rate of 200:4 and 300:2, respectively due to cells bridging within the bundles of microfibers.

4. CONCLUSION

Aligned PCL microfibers with different features were fabricated in this study using microfluidic fiber fabrication. The mean diameter of the fabricated fibers ranged from 2.6 to 36.5 μm by selecting the sheath-to-core flow rate ratio from 400:1 to 20:5. The mean deviation angles (±standard error) were found 3.95 ± 0.70, 4.64 ± 0.51, 3.84 ± 0.50, 4.39 ± 0.54, and 4.88 ± 0.62 for the sheath-to-core flow rates of 20:5, 60:5, 200:4, 300:2, and 400:1, respectively. The fibers were coated with a complex extracellular matrix substrate via physical absorption to facilitate cell attachment and for guiding the direction of AHPC growth in vitro. The results showed that the PCL fiber can be used as a fibrous scaffold which is not cytotoxic to the AHPCs, and supports cell adhesion, differentiation, and proliferation. Additionally, it was shown that the clusters of these adult neural stem cells can be aligned using the PCL microfibers. The quantitative analysis demonstrated that the cell deviation angle for most of the cells guided by different types of fibers was less than 10°. On average, 58% of the cells in all types of the fibers had a cell deviation angle less than 10°, revealing the functionality and potential of the PCL microfibers for guiding nerve regeneration within the central (CNS) and peripheral nervous system (PNS) and may facilitate repair of spinal cord injuries (SCI) and peripheral nerve injuries (PNI). This integration of multiple cues within a 3D context is important for gaining a better understanding in regulating neural stem cell differentiation and in designing scaffolds for neural tissue engineering. We are currently implanting bundles of PCL microfibers into conduits, and the preliminary results suggest that this approach may aid in regeneration of severed nerve injuries. By mimicking the microenvironment of the nervous system, regeneration can be enhanced due to biological and chemical cues in the environment. Using conduits with PCL microfiber bundles can be investigated for various regeneration strategies including central nervous system diseases in order to repair a damaged system. In addition, the PCL fibers can be applied in regeneration of other tissues such as muscle, tendons, and blood vessels.

■ ASSOCIATED CONTENT

Supporting Information

The Supporting Information is available free of charge on the ACS Publications website at DOI: 10.1021/acs.biomac.6b01028.

Detailed information about the dimensions of the microchannel, preparation of PCL fibrous scaffold, proliferation of AHPCs on PCL fibers with different sizes, neural differentiation of AHPCs on PCL fibers, and primary antibody information (PDF)

■ AUTHOR INFORMATION

Corresponding Author

*E-mail: nastaran@iastate.edu.

Notes

The authors declare no competing financial interest.

■ ACKNOWLEDGMENTS

This work was supported by the Office of Naval Research Grant N000141612246, Iowa State University Presidential Initiative for Interdisciplinary Research, US Army Medical Research and Materiel Command, and the Stem Cell Research Fund. The authors would also like to thank Kurt Koch for his help in coating the samples for SEM and Ashley Christopherson for illustrating the microfluidic fiber fabrication approach.

■ REFERENCES

(1) Langer, R.; Vacanti, J. Tissue engineering. *Science* **1993**, *260*, 920−926.

(2) Caplin, J. D.; Granados, N. G.; James, M. R.; Montazami, R.; Hashemi, N. Microfluidic Organ-on-a-Chip Technology for Advancement of Drug Development and Toxicology. *Adv. Healthcare Mater.* **2015**, *4*, 1426−1450.

(3) Andersson, H.; Berg, A.v.d. Microfabrication and microfluidics for tissue engineering: state of the art and future opportunities. *Lab Chip* **2004**, *4*, 98−103.

(4) Khademhosseini, A.; Langer, R.; Borenstein, J.; Vacanti, J. P. Microscale technologies for tissue engineering and biology. *Proc. Natl. Acad. Sci. U. S. A.* **2006**, *103*, 2480−2487.

(5) Daniele, M. A.; Boyd, D. A.; Adams, A. A.; Ligler, F. S. Microfluidic Strategies for Design and Assembly of Microfibers and Nanofibers with Tissue Engineering and Regenerative Medicine Applications. *Adv. Healthcare Mater.* **2015**, *4*, 2.

(6) Deshayes, S.; Kasko, A. M. Polymeric biomaterials with engineered degradation. *J. Polym. Sci., Part A: Polym. Chem.* **2013**, *51*, 3531−3566.

(7) Acar, H.; Çınar, S.; Thunga, M.; Kessler, M. R.; Hashemi, N.; Montazami, R. Study of Physically Transient Insulating Materials as a Potential Platform for Transient Electronics and Bioelectronics. *Adv. Funct. Mater.* **2014**, *24*, 4135−4143.

(8) Schmidt, C. E.; Leach, J. B. Neural Tissue Engineering: Strategies for Repair and Regeneration. *Annu. Rev. Biomed. Eng.* **2003**, *5*, 293−347.

(9) Hurtado, A.; Cregg, J. M.; Wang, H. B.; Wendell, D. F.; Oudega, M.; Gilbert, R. J.; McDonald, J. W. Robust CNS regeneration after complete spinal cord transection using aligned poly-l-lactic acid microfibers. *Biomaterials* **2011**, *32*, 6068−6079.

(10) Rodda, A. E.; Ercole, F.; Glattauer, V.; Gardiner, J.; Nisbet, D. R.; Healy, K. E.; Forsythe, J. S.; Meagher, L. Low Fouling Electrospun Scaffolds with Clicked Bioactive Peptides for Specific Cell Attachment. *Biomacromolecules* **2015**, *16*, 2109−2118.

(11) Viswanathan, P.; Themistou, E.; Ngamkham, K.; Reilly, G. C.; Armes, S. P.; Battaglia, G. Controlling Surface Topology and Functionality of Electrospun Fibers on the Nanoscale using

DOI: 10.1021/acs.biomac.6b01028
Biomacromolecules 2016, 17, 3287−3297

Amphiphilic Block Copolymers To Direct Mesenchymal Progenitor Cell Adhesion. *Biomacromolecules* **2015**, *16*, 66−75.
(12) Zhu, B.; Li, W.; Lewis, R. V.; Segre, C. U.; Wang, R. E-Spun Composite Fibers of Collagen and Dragline Silk Protein: Fiber Mechanics, Biocompatibility, and Application in Stem Cell Differentiation. *Biomacromolecules* **2015**, *16*, 202−213.
(13) Hwang, C. M.; Khademhosseini, A.; Park, Y.; Sun, K.; Lee, S.-H. Microfluidic Chip-Based Fabrication of PLGA Microfiber Scaffolds for Tissue Engineering. *Langmuir* **2008**, *24*, 6845−6851.
(14) Kang, E.; Choi, Y. Y.; Chae, S.-K.; Moon, J.-H.; Chang, J.-Y.; Lee, S.-H. Microfluidic Spinning of Flat Alginate Fibers with Grooves for Cell-Aligning Scaffolds. *Adv. Mater.* **2012**, *24*, 4271−4277.
(15) Siriwardane, M. L.; DeRosa, K.; Collins, G.; Pfister, B. J. Controlled formation of cross-linked collagen fibers for neural tissue engineering applications. *Biofabrication* **2014**, *6*, 015012.
(16) Gnavi, S.; Fornasari, B. E.; Tonda-Turo, C.; Ciardelli, G.; Zanetti, M.; Geuna, S.; Perroteau, I. The influence of electrospun fibre size on Schwann cell behaviour and axonal outgrowth. *Mater. Sci. Eng., C* **2015**, *48*, 620−631.
(17) Kador, K. E.; Montero, R. B.; Venugopalan, P.; Hertz, J.; Zindell, A. N.; Valenzuela, D. A.; Uddin, M. S.; Lavik, E. B.; Muller, K. J.; Andreopoulos, F. M.; Goldberg, J. L. Tissue engineering the retinal ganglion cell nerve fiber layer. *Biomaterials* **2013**, *34*, 4242−4250.
(18) Mu, Y.; Wu, F.; Wei, Y. L. L.; Yuan, W. Progress of electrospun fibers as nerve conduits for neural tissue repair. *Nanomedicine* **2014**, *9*, 1869−1883.
(19) Tamayol, A.; Akbari, M.; Annabi, N.; Paul, A.; Khademhosseini, A.; Juncker, D. Fiber-based tissue engineering: Progress, challenges, and opportunities. *Biotechnol. Adv.* **2013**, *31*, 669−687.
(20) Agarwal, S.; Wendorff, J. H.; Greiner, A. Use of electrospinning technique for biomedical applications. *Polymer* **2008**, *49*, 5603−5621.
(21) Schnell, E.; Klinkhammer, K.; Balzer, S.; Brook, G.; Klee, D.; Dalton, P.; Mey, J. Guidance of glial cell migration and axonal growth on electrospun nanofibers of poly-ε-caprolactone and a collagen/poly-ε-caprolactone blend. *Biomaterials* **2007**, *28*, 3012−3025.
(22) Ghasemi-Mobarakeh, L.; Prabhakaran, M. P.; Morshed, M.; Nasr-Esfahani, M. H.; Ramakrishna, S. Electrospun poly(epsilon-caprolactone)/gelatin nanofibrous scaffolds for nerve tissue engineering. *Biomaterials* **2008**, *29*, 4532−4539.
(23) Fioretta, E. S.; Simonet, M.; Smits, A. I. P. M.; Baaijens, F. P. T.; Bouten, C. V. C. Differential Response of Endothelial and Endothelial Colony Forming Cells on Electrospun Scaffolds with Distinct Microfiber Diameters. *Biomacromolecules* **2014**, *15*, 821−829.
(24) Wang, X.; Salick, M. R.; Wang, X.; Cordie, T.; Han, W.; Peng, Y.; Li, Q.; Turng, L.-S. Poly(ε-caprolactone) Nanofibers with a Self-Induced Nanohybrid Shish-Kebab Structure Mimicking Collagen Fibrils. *Biomacromolecules* **2013**, *14*, 3557−3569.
(25) Leung, M.; Cooper, A.; Jana, S.; Tsao, C.-T.; Petrie, T. A.; Zhang, M. Nanofiber-Based in Vitro System for High Myogenic Differentiation of Human Embryonic Stem Cells. *Biomacromolecules* **2013**, *14*, 4207−4216.
(26) Cooper, A.; Bhattarai, N.; Zhang, M. Fabrication and cellular compatibility of aligned chitosan−PCL fibers for nerve tissue regeneration. *Carbohydr. Polym.* **2011**, *85*, 149−156.
(27) Nisbet, D. R.; Yu, L. M. Y.; Zahir, T.; Forsythe, J. S.; Shoichet, M. S. Characterization of neural stem cells on electrospun poly(ε-caprolactone) submicron scaffolds: evaluating their potential in neural tissue engineering. *J. Biomater. Sci., Polym. Ed.* **2008**, *19*, 623−634.
(28) Daud, M. F. B.; Pawar, K. C.; Claeyssens, F.; Ryan, A. J.; Haycock, J. W. An aligned 3D neuronal-glial co-culture model for peripheral nerve studies. *Biomaterials* **2012**, *33*, 5901−5913.
(29) Li, D.; Chen, W.; Sun, B.; Li, H.; Wu, T.; Ke, Q.; Huang, C.; El-Hamshary, H.; Al-Deyab, S. S.; Mo, X. A comparison of nanoscale and multiscale PCL/gelatin scaffolds prepared by disc-electrospinning. *Colloids Surf., B* **2016**, *146*, 632−641.
(30) Omidvar, N.; Ganji, F.; Eslaminejad, M. B. In vitro osteogenic induction of human marrow-derived mesenchymal stem cells by PCL fibrous scaffolds containing dexamethazone-loaded chitosan microspheres. *J. Biomed. Mater. Res., Part A* **2016**, *104*, 1657−1667.
(31) Jung, J. H.; Choi, C. H.; Chung, S.; Chung, Y. M.; Lee, C. S. Microfluidic synthesis of a cell adhesive Janus polyurethane microfiber. *Lab Chip* **2009**, *9*, 2596−2602.
(32) Sharifi, F.; Sooriyarachchi, A. C.; Altural, H.; Montazami, R.; Rylander, M. N.; Hashemi, N. Fiber Based Approaches as Medicine Delivery Systems. *ACS Biomater. Sci. Eng.* **2016**, *2*, 1411.
(33) Han, L.-H.; Yu, S.; Wang, T.; Behn, A. W.; Yang, F. Microribbon-Like Elastomers for Fabricating Macroporous and Highly Flexible Scaffolds that Support Cell Proliferation in 3D. *Adv. Funct. Mater.* **2013**, *23*, 346−358.
(34) Leonor, I. B.; Rodrigues, M. T.; Gomes, M. E.; Reis, R. L. In situ functionalization of wet-spun fibre meshes for bone tissue engineering. *J. Tissue Eng. Regener. Med.* **2011**, *5*, 104−111.
(35) Bai, Z. H.; Reyes, J. M. M.; Montazami, R.; Hashemi, N. On-chip development of hydrogel microfibers from round to square/ribbon shape. *J. Mater. Chem. A* **2014**, *2*, 4878−4884.
(36) Lee, C.-Y.; Wang, W.-T.; Liu, C.-C.; Fu, L.-M. Passive mixers in microfluidic systems: A review. *Chem. Eng. J.* **2016**, *288*, 146−160.
(37) Yang, J.; Ghobadian, S.; Goodrich, P. J.; Montazami, R.; Hashemi, N. Miniaturized biological and electrochemical fuel cells: challenges and applications. *Phys. Chem. Chem. Phys.* **2013**, *15*, 14147−14161.
(38) Sharifi, F.; Ghobadian, S.; Cavalcanti, F. R.; Hashemi, N. Paper-based devices for energy applications. *Renewable Sustainable Energy Rev.* **2015**, *52*, 1453−1472.
(39) Hashemi, N.; Lackore, J. M.; Sharifi, F.; Goodrich, P. J.; Winchell, M. L.; Hashemi, N. A paper-based microbial fuel cell operating under continuous fl ow condition. *Technology* **2016**, *4*, 98−103.
(40) Shi, X.; Ostrovidov, S.; Zhao, Y.; Liang, X.; Kasuya, M.; Kurihara, K.; Nakajima, K.; Bae, H.; Wu, H.; Khademhosseini, A. Microfluidic Spinning of Cell-Responsive Grooved Microfibers. *Adv. Funct. Mater.* **2015**, *25*, 2250−2259.
(41) Daniele, M. A.; Adams, A. A.; Naciri, J.; North, S. H.; Ligler, F. S. Interpenetrating networks based on gelatin methacrylamide and PEG formed using concurrent thiol click chemistries for hydrogel tissue engineering scaffolds. *Biomaterials* **2014**, *35*, 1845−1856.
(42) Goodrich, P. J.; Sharifi, F.; Hashemi, N. Rapid prototyping of microchannels with surface patterns for fabrication of polymer fibers. *RSC Adv.* **2015**, *5*, 71203−71209.
(43) Jun, Y.; Kang, E.; Chae, S.; Lee, S. H. Microfluidic spinning of micro- and nano-scale fibers for tissue engineering. *Lab Chip* **2014**, *14*, 2145−2160.
(44) Daniele, M. A.; Radom, K.; Ligler, F. S.; Adams, A. A. Microfluidic fabrication of multiaxial microvessels via hydrodynamic shaping. *RSC Adv.* **2014**, *4*, 23440−23446.
(45) Sharifi, F.; Kurteshi, D.; Hashemi, N. Designing highly structured polycaprolactone fibers using microfluidics. *J. Mech. Behav. Biomed. Mater.* **2016**, *61*, 530−540.
(46) Sharifi, F.; Bai, Z.; Montazami, R.; Hashemi, N. Mechanical and physical properties of poly(vinyl alcohol) microfibers fabricated by a microfluidic approach. *RSC Adv.* **2016**, *6*, 55343−55353.
(47) Daniele, M. A.; North, S. H.; Naciri, J.; Howell, P. B.; Foulger, S. H.; Ligler, F. S.; Adams, A. A. Rapid and Continuous Hydrodynamically Controlled Fabrication of Biohybrid Microfibers. *Adv. Funct. Mater.* **2013**, *23*, 698−704.
(48) Lin, Y. S.; Huang, K. S.; Yang, C. H.; Wang, C. Y.; Yang, Y. S.; Hsu, H. C.; Liao, Y. J.; Tsai, C. W. Microfluidic Synthesis of Microfibers for Magnetic-Responsive Controlled Drug Release and Cell Culture. *PLoS One* **2012**, *7*, e33184.
(49) Hasani-Sadrabadi, M. M.; VanDersarl, J. J.; Dashtimoghadam, E.; Bahlakeh, G.; Majedi, F. S.; Mokarram, N.; Bertsch, A.; Jacob, K. I.; Renaud, P. A microfluidic approach to synthesizing high-performance microfibers with tunable anhydrous proton conductivity. *Lab Chip* **2013**, *13*, 4549−4553.
(50) Raof, N. A.; Padgen, M. R.; Gracias, A. R.; Bergkvist, M.; Xie, Y. B. One-dimensional self-assembly of mouse embryonic stem cells using an array of hydrogel microstrands. *Biomaterials* **2011**, *32*, 4498−4505.

DOI: 10.1021/acs.biomac.6b01028
Biomacromolecules 2016, 17, 3287−3297

(51) Kang, E.; Jeong, G. S.; Choi, Y. Y.; Lee, K. H.; Khademhosseini, A.; Lee, S. H. Digitally tunable physicochemical coding of material composition and topography in continuous microfibres. *Nat. Mater.* **2011**, *10*, 877−883.
(52) Choi, C. H.; Yi, H.; Hwang, S.; Weitz, D. A.; Lee, C. S. Microfluidic fabrication of complex-shaped microfibers by liquid template-aided multiphase microflow. *Lab Chip* **2011**, *11*, 1477−1483.
(53) Boyd, D. A.; Shields, A. R.; Howell, P. B.; Ligler, F. S. Design and fabrication of uniquely shaped thiol-ene microfibers using a two-stage hydrodynamic focusing design. *Lab Chip* **2013**, *13*, 3105−3110.
(54) Cho, S.; Shim, T. S.; Yang, S. M. High-throughput optofluidic platforms for mosaicked microfibers toward multiplex analysis of biomolecules. *Lab Chip* **2012**, *12*, 3676−3679.
(55) Patenaude, M.; Hoare, T. Injectable, Mixed Natural-Synthetic Polymer Hydrogels with Modular Properties. *Biomacromolecules* **2012**, *13*, 369−378.
(56) Middleton, J. C.; Tipton, A. J. Synthetic biodegradable polymers as orthopedic devices. *Biomaterials* **2000**, *21*, 2335−2346.
(57) Wong, D. Y.; Hollister, S. J.; Krebsbach, P. H.; Nosrat, C. Poly(ε-Caprolactone) and Poly (L-Lactic-Co-Glycolic Acid) Degradable Polymer Sponges Attenuate Astrocyte Response and Lesion Growth in Acute Traumatic Brain Injury. *Tissue Eng.* **2007**, *13*, 2515−2523.
(58) Mahapatro, A.; Singh, D. K. Biodegradable nanoparticles are excellent vehicle for site directed in-vivo delivery of drugs and vaccines. *J. Nanobiotechnol.* **2011**, *9*, 55.
(59) Woodruff, M. A.; Hutmacher, D. W. The return of a forgotten polymer—Polycaprolactone in the 21st century. *Prog. Polym. Sci.* **2010**, *35*, 1217−1256.
(60) Recknor, J. B.; Sakaguchi, D. S.; Mallapragada, S. K. Directed growth and selective differentiation of neural progenitor cells on micropatterned polymer substrates. *Biomaterials* **2006**, *27*, 4098−4108.
(61) Oh, J.; Daniels, G. J.; Chiou, L. S.; Ye, E.-A.; Jeong, Y.-S.; Sakaguchi, D. S. Multipotent adult hippocampal progenitor cells maintained as neurospheres favor differentiation toward glial lineages. *Biotechnol. J.* **2014**, *9*, 921−933.
(62) Gage, F. H.; Coates, P. W.; Palmer, T. D.; Kuhn, H. G.; Fisher, L. J.; Suhonen, J. O.; Peterson, D. A.; Suhr, S. T.; Ray, J. Survival and differentiation of adult neuronal progenitor cells transplanted to the adult brain. *Proc. Natl. Acad. Sci. U. S. A.* **1995**, *92*, 11879−11883.
(63) Hashemi, N.; Erickson, J. S.; Golden, J. P.; Jackson, K. M.; Ligler, F. S. Microflow Cytometer for optical analysis of phytoplankton. *Biosens. Bioelectron.* **2011**, *26*, 4263−4269.
(64) Hashemi, N.; Erickson, J. S.; Golden, J. P.; Ligler, F. S. Optofluidic characterization of marine algae using a microflow cytometer. *Biomicrofluidics* **2011**, *5*, 032009.
(65) Hashemi, N.; Howell, P. B., Jr.; Erickson, J. S.; Golden, J. P.; Ligler, F. S. Dynamic reversibility of hydrodynamic focusing for recycling sheath fluid. *Lab Chip* **2010**, *10*, 1952−1959.

DOI: 10.1021/acs.biomac.6b01028
Biomacromolecules 2016, 17, 3287−3297